ChemPubSoc Europe

DOI: 10.1002/cphc.201500504

CHEMPHYSCHEM Articles

Theoretical Insights into the Tuning of Metal Binding Sites of Paddlewheels in *rht*-Metal–Organic Frameworks

Tony Pham,* Katherine A. Forrest, Wen-Yang Gao, Shengqian Ma, and Brian Space[a]

Theoretical investigations of CO_2 sorption are performed in four members of the highly tunable *rht*-metal–organic framework (MOF) platform. *rht*-MOFs contain two Cu^{2+} ions that comprise the metal paddlewheels and both are in chemically distinct environments. Indeed, one type of Cu^{2+} ion faces toward the center of the linker whereas the other type faces away from the center of the linker. Electronic structure calculations on the series of *rht*-MOFs demonstrate that one of the Cu^{2+} ions has a consistently higher charge magnitude relative to the other. As a consequence, the Cu^{2+} ion with the higher partial positive charge acts as the favored sorbate binding site at initial loading as revealed by grand canonical Monte Carlo (GCMC) simulations that include many-body polarization. It was found that the charge distribution about the copper paddlewheels is dependent on the type of functional groups present on the linker. This study demonstrates how the binding site about the metal paddlewheels in the *rht*-MOF platform can be controlled by changing the functionality on the organic ligand.

1. Introduction

Metal–organic frameworks (MOFs) are an increasingly important class of porous materials that are comprised of organic ligands coordinated to metal-ion clusters.[1–6] They have promising potential for a variety of applications, including gas storage,[7–13] gas separations,[14–20] catalysis,[21–25] sensing,[26–28] drug delivery,[29–31] magnetism,[32,33] electrical conductivity,[34,35] and nonlinear optics.[36–38] MOFs can be synthesized to have moderate to high surface areas and can be assembled from molecular building blocks (MBB) with desired/tunable chemical functionality.[9,39] The building block approach allows for the possibility to create a vast number of MOF structures.[2,40]

A highly successful platform of MOFs that has been synthesized are the (3,24)-connected *rht*-MOFs.[9,41–69] These MOFs are synthesized with hexatopic ligands consisting of three coplanar isophthalate moieties that are coordinated to $[M_2(O_2CR)_4]$ square paddlewheel clusters. The overall structure of *rht*-MOFs is characterized by having 24 edges of a cuboctahedron connecting with a hexatopic ligand having C_3 symmetry. Moreover, the overall framework of *rht*-MOFs consists of three distinct cages: cuboctahedron, truncated tetrahedron, and truncated octahedron (see Figure S1, Supporting Information, SI). *rht*-MOFs are a promising platform of MOFs because they exhibit very high surface areas, contain open-metal sites, and have tunable pores and functionality. They have been shown to exhibit high uptake capacities for energy-related gases, such H_2, CO_2, and CH_4.

The first *rht*-MOF, known as *rht*-MOF-1, was synthesized by Nouar et al. in 2008.[41] It was constructed using trigonal Cu_3O trimers linked to 5-tetrazolylisophthalate moieties that serve as the hexatopic building block, which in turn are coordinated to Cu^{2+} ions to form the $[Cu_2(O_2CR)_4]$ (copper paddlewheel) clusters. Furthermore, the MOF contains nitrate counterions to balance the charge of the cationic framework. *rht*-MOF-1 has an estimated BET surface area of 2847 $m^2 g^{-1}$ (Langmuir surface area = 3223 $m^2 g^{-1}$), a pore volume of 1.01 $cm^3 g^{-1}$, and a free volume of approximately 75%. Experimental studies have demonstrated that *rht*-MOF-1 has a high hydrogen uptake of 2.4 wt% at 77 K and 1.0 atm, where wt% is defined as: [(mass of H_2)/(mass of MOF + mass of H_2)] × 100%.

Recently, an isostructural analogue of *rht*-MOF-1 was constructed by substituting 5-tetrazolylisophthalate with 5-(1H-pyrazol-4-yl)isophthalate; this alteration replaces the carbon-coordinated N atoms of the five-membered ring by C-H groups.[68] This MOF, known as MPAF-1 (MPAF stands for metal-pyrazolate framework) or *rht*-MOF-pyr, exhibits a similar surface area, pore volume, and free volume as *rht*-MOF-1, but displays a much higher stability in water, moisture, steam, and acid. As demonstrated in previous computational studies, this improved stability can be attributed to the increase in the electron density of the copper-coordinated N atoms, which resulted in stronger bonds with the Cu^{2+} ions of the Cu_3O trimers, in addition to the increase in the stability about the copper paddlewheels.[68]

Although the aforementioned MOFs are examples of *rht*-MOFs that were synthesized using the Cu_3O trimer units,[56,68] many other *rht*-MOFs have been constructed such that it avoids the utilization of such moieties. An example of such an *rht*-MOF is PCN-61 (PCN stands for porous coordination network).[45,46,70] This *rht*-MOF is composed of 5,5′,5″-benzene-

[a] *Dr. T. Pham,[+] K. A. Forrest,[+] W.-Y. Gao, Prof. S. Ma, Prof. B. Space*
Department of Chemistry, University of South Florida, 4202 E. Fowler Ave., CHE205, Tampa, FL 33620-5250 (USA)
E-mail: tpham4@mail.usf.edu

[+] *These authors contributed equally.*

Supporting Information for this article is available on the WWW under http://dx.doi.org/10.1002/cphc.201500504.

1,3,5-triyltris(1-ethynl-2-isophthalate) (btei) linkers coordinated to Cu^{2+} ions. The MOF has an estimated BET surface area of 3000 $m^2 g^{-1}$ (Langmuir surface area = 3500 $m^2 g^{-1}$), a pore volume of 1.36 $cm^3 g^{-1}$, and a free volume of approximately 77%. Experimental studies have shown that PCN-61 has a hydrogen uptake of 2.25 wt% at 77 K and 1.0 atm.[46] Moreover, PCN-61 exhibited an excess CO_2 uptake of 3.15 mmol g^{-1} at 298 K and 1.0 atm.[48]

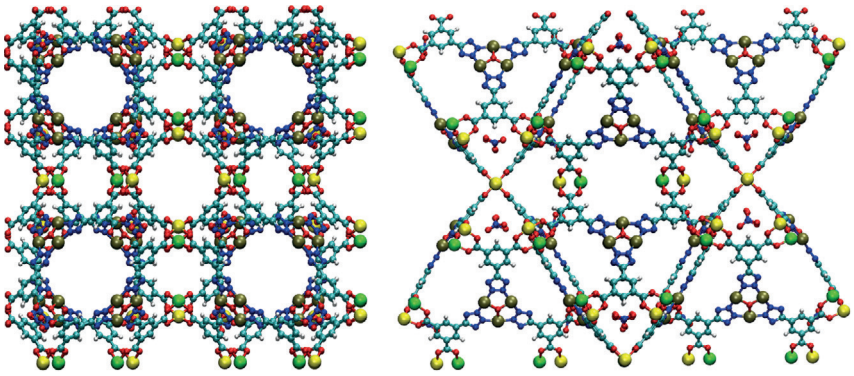

Figure 1. a) Side view and b) corner view of a unit cell of *rht*-MOF-1. The Cu^{2+} ions colored in green are denoted as Cu1, while the Cu^{2+} ions colored in yellow are denoted as Cu2. The same labeling for the Cu^{2+} ions on the paddlewheel can be made for other *rht*-MOFs. Atom colors: C = cyan, H = white, N = blue, O = red, Cu = green/yellow/tan.

Recently, an *rht*-MOF was synthesized that resembled an improvement over PCN-61 in terms of functionality and gas uptake capacity; it is referred to as Cu-TPBTM.[48] This *rht*-MOF was constructed with *N*,*N*′*N*″-tris(isophthalyl)-1,3,5-benzenetricarboxamide (TPBTM) as the organic linker. In essence, Cu-TPBTM contains polar amide groups in place of the nonpolar alkyne groups that are seen in PCN-61. This MOF displayed a similar surface area, pore volume, and free volume as PCN-61; however, Cu-TPBTM exhibited a drastically higher uptake for H_2 and CO_2 as a result of the increased functionality through the amide groups. For H_2 sorption at 77 K and 1.0 atm and CO_2 sorption at 298 K and 1.0 atm, the corresponding gas uptakes for Cu-TPBTM were 2.61 wt% and 5.29 mmol g^{-1}, respectively.[48,71] These H_2 and CO_2 uptake values are among the highest for all *rht*-MOFs.

Indeed, a number of *rht*-MOFs have been synthesized by simply changing the functionality on the hexatopic ligands. Although all MOFs within this platform have the same structural motif, each *rht*-MOF has different chemical properties, which are dependent on the moieties on the ligands that they contain. Note, all organic ligands and metal paddlewheels are equivalent to each other within the crystal structure of *rht*-MOFs. Considering the three cages that comprise all *rht*-MOFs, each metal paddlewheel simultaneously serves as the corner of the triangular windows of the cuboctahedral and truncated tetrahedral cages as well as the square windows of the cuboctahedral and truncated octahedral cages. Similarly, each ligand serves as a side of the truncated tetrahedral and truncated octahedral cages, with the heads of the ligand joining the windows of the cuboctahedral cages.

In this work, we will show through theoretical studies that the sorbate binding site about the metal paddlewheels in the *rht*-MOF platform are also electronically tunable, that is, the binding site can be controlled by simply changing the functionality on the ligand and consequently the metal electropositivity. Here, the focus is on CO_2 sorption in *rht*-MOFs, although the same trends can be observed for other sorbates, such as H_2,[70,71] because the controlling factor is the metal partial charge. Specifically, the key factor that governs the sorbate binding site about the metal paddlewheels is the electrostatics about the Cu^{2+} ions that comprise these paddlewheels. It is important to emphasize that the two Cu^{2+} ions within the Cu paddlewheels in all *rht*-MOFs are in chemically distinct environments. This is due to the fact that the carboxylate carbon-aromatic carbon bond cannot rotate freely in the MOF environment. One of the Cu^{2+} ions faces toward the center of the linker and projects into the truncated tetrahedral and truncated octahedral cages; it is referred to herein as Cu1 (green colored Cu^{2+} ions in Figure 1; atom label 1 in Figure S2–S5). The other Cu^{2+} ion faces away from the center of the linker and projects into the cuboctahedral cages; it is referred to herein as Cu2 (yellow colored Cu^{2+} ions in Figure 1; atom label 2 in Figures S2–S5). The notion that there are two types of Cu^{2+} ions on the paddlewheels in all *rht*-MOFs was supported by experimental neutron powder diffraction (NPD) studies of D_2 sorption in the MOF NOTT-112, where it was observed that the D_2 molecules sorb mostly onto the Cu2 ions at low loading and not the other type of Cu^{2+} ion; this provided an overall distinction between the two types of Cu^{2+} ions on the paddlewheels in *rht*-MOFs.[47]

In certain previous computational studies by other groups on *rht*-MOFs,[9,60,72,73] the two Cu^{2+} ions about the Cu paddlewheels were treated in a mean field fashion as chemically equivalent. As a result, they were assigned the same point partial charges in the force field for MOF-sorbate simulation studies. Although these Cu^{2+} ions are not identical, it is conceivable that they might be similar because *rht*-MOFs have a topology that is similar to that of HKUST-1, a MOF consisting of 1,3,5-benzenetricarboxylate ligands coordinated to Cu paddlewheel units.[74] In HKUST-1, all Cu^{2+} ions in the structure are equivalent to each other. However, as explained above, this is not the case in *rht*-MOFs. Unfortunately, treating the Cu^{2+} ions as chemically equivalent in *rht*-MOFs resulted in only a small occupation of sorbate molecules about the open-metal sites for the MOF-sorbate simulations even though the simulated sorption isotherms were in reasonable agreement with experiment.[60,72,73] As a result, in some previous studies, the correct chemistry between the sorbate molecules and the unsaturated metal centers was not captured, pointing to the difficulty in using just sorption data in comparing theoretical and experimental results. Reproducing measured isotherms is encourag-

ing, but not sufficient nor strictly necessary for a reasonable MOF-sorbate model. Note, the experimental initial isosteric heats of adsorption (Q_{st}) values and existing Cu^{2+}-sorbate interaction distances inferred from neutron scattering studies confirm strong sorbate binding to the metal sites.[47,75–77] Capturing this effect in simulation requires both the proper parametrization of the Cu^{2+} ions and the inclusion of explicit polarization.

As shown in previous modeling studies,[70,71,78–83] the inclusion of explicit polarization interactions was necessary for describing sorption onto the open-metal sites. This was demonstrated using highly accurate and transferable potentials that included such interactions.[84–88] Indeed, for simulations in highly charged/polar MOFs, the effects of many-body polarization resulted in sorption isotherms and loading dependent Q_{st} values in agreement with experiment as well as capturing the critical interaction between the sorbate molecules and the polarizable metal centers, leading to characteristic metal–sorbate distances. Potential energy functions including only explicit charge–quadrupole interactions and polarization implemented through an implicit fashion were not sufficient to describe the correct sorption behavior in such MOFs. For this work, we used a recently developed and extensively tested CO_2 potential that includes explicit induced dipole interactions for the purpose of simulating in heterogeneous media.[85] As demonstrated later, simulations using this model will result in a significant occupancy of CO_2 molecules onto the open-metal sites at low loading.

Note, many theoretical groups use the TraPPE CO_2 potential[89] to model CO_2 sorption in MOFs. Although this model is an excellent bulk potential that was fit to vapor–liquid equilibria, it typically does not perform consistently well in describing the sorbate intermolecular interactions in heterogeneous media. This is especially for highly charged/polar MOFs that have polarizable sites. It will be shown that simulations of CO_2 sorption using the TraPPE model in such MOFs lead to sorption to regions that are dominated by van der Waals and charge–quadrupole energetics and not to those that are dominated by induction.

Because the two Cu^{2+} ions about the Cu paddlewheels are chemically distinct in *rht*-MOFs, the relative point partial charges about each ion are different. Specifically, one type of Cu^{2+} ion is found to have a higher partial positive charge than the other. The difference in relative charge magnitudes have been shown to be significant for simulations of gas sorption in *rht*-MOFs, with the more positive Cu^{2+} ion acting as the favored sorption site while the lower charged Cu^{2+} ion shows little interaction with the sorbates under moderate conditions.[70,71,79,80,90] Typically, the Cu2 ions would have the higher partial positive charge as shown empirically in previous computational studies in *rht*-MOFs.[68,70] These types of Cu^{2+} ions are located in what has been observed to be a more favorable chemical environment (projecting into the cuboctahedral cages). An example of an *rht*-MOF that would exhibit this electrostatic behavior for the Cu^{2+} ions is PCN-61.[70] However, by changing the functional group on the organic ligand to one that is polar or electron withdrawing, the electrostatics about the Cu^{2+} ions of the paddlewheels can be reversed, that is, the introduction of such moieties would cause the Cu1 ions to have the greater positive charge. This effect can be seen in Cu-TPBTM, which is an isostructural analogue to PCN-61.[71] In Cu-TPBTM, the presence of the negatively charged oxygen atom of the amide group causes the Cu1 ions to exhibit a higher partial positive charge through an inductive effect. Essentially, the type of functional group that is present on the organic linker in *rht*-MOFs has an effect on the electrostatics of the Cu^{2+} ions about the paddlewheels, and therefore, the initial binding sites by altering the relative binding enthalpies.

In this work, we use grand canonical Monte Carlo (GCMC) methods to investigate CO_2 sorption in four *rht*-MOFs: *rht*-MOF-1, MPAF-1, PCN-61, and Cu-TPBTM. The organic ligands for all four *rht*-MOFs are shown in Figure 2. It will be shown that substituting 5-tetrazolylisophthalate as seen in rht-MOF-1 with 5-(1H-pyrazol-4-yl)isophthalate as observed in MPAF-1 will cause the initial CO_2 binding site to change from the Cu1 ions to the Cu2 ions at low loading. Similarly, substituting the alkyne functional groups that are seen in PCN-61 with amide functional groups as observed in Cu-TPBTM will result

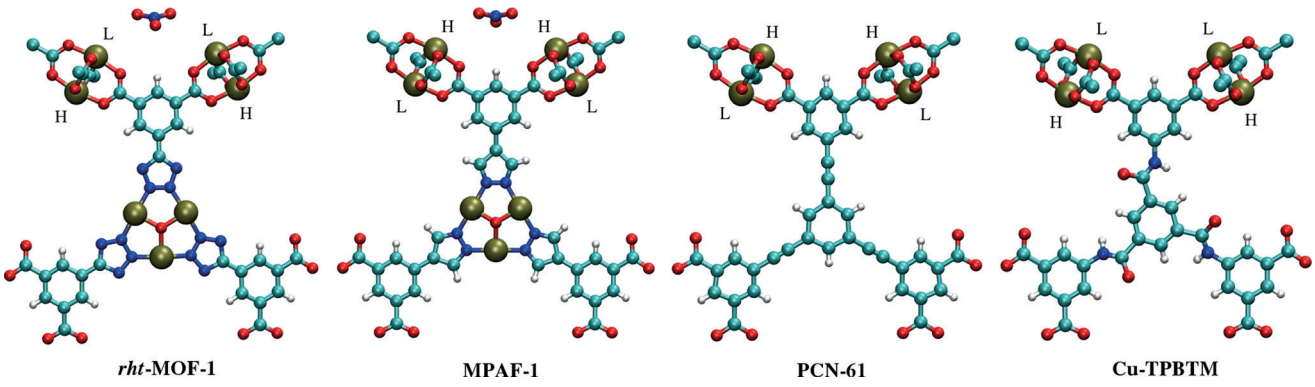

Figure 2. The organic ligand and copper paddlewheel units in *rht*-MOF-1, MPAF-1, PCN-61, and Cu-TPBTM. "H" denotes the Cu^{2+} ion on the paddlewheel that exhibits the higher partial positive charge, while "L" denotes the Cu^{2+} ion on the paddlewheel that exhibits the lower partial positive charge. Atom colors: C = cyan, H = white, N = blue, O = red, Cu = tan.

in the sorbate binding site to switch from the Cu2 ions to the Cu1 ions. This will be confirmed by examining the radial distribution functions, $g(r)$, of CO_2 molecules about the Cu1 and Cu2 ions, the three-dimensional histograms showing the initial sites of metal paddlewheel sorption, and molecular illustrations of the CO_2 binding site about the Cu paddlewheels in all *rht*-MOFs. In essence, the initial metal binding site in *rht*-MOFs can be tuned by making a simple change in the organic linker. This allows for the possibility for rational design in synthesis where experimentalists can tune which site they want the sorbate to bind to at initial loading by making a simple chemical modification in the ligand. Such straightforward control of the metal site electronics in the condensed phase could be useful for a variety of applications beyond sorption, such as catalysis and those involving electron transfer.

Methods

All parametrizations and simulations of CO_2 sorption in *rht*-MOF-1, MPAF-1, PCN-61, and Cu-TPBTM were performed on a single unit cell of the crystallographic structure of the respective *rht*-MOFs; these were taken from refs. [41], [68], [45], and [48], respectively. For the simulations of all four *rht*-MOFs, Lennard-Jones 12-6 parameters, atomic point partial charges, and atomic point polarizabilities were assigned to the nuclear centers of all atoms of the respective frameworks. This was done to capture the corresponding van der Waals repulsion/dispersion, stationary electrostatic, and induced dipole energetics in simulation. The Lennard-Jones parameters for all atoms were taken from the Universal Force Field (UFF).[91] This set of Lennard-Jones parameters was widely used in computational MOF studies performed earlier,[72,78,92–95] and was shown to reproduce high temperature/pressure isotherms for hydrogen in IRMOF-1 in particular.[96] To model explicit polarization, all C, H, N, and O atoms were assigned the exponential point polarizability parameters as determined by van Duijnen et al.[97] This set of polarizability parameters was carefully parametrized and had been shown to be highly transferable.[70,71,78–83,90,98–106] The polarizability parameter for Cu^{2+} was determined in previous work[70] and was also considered in this work. For each *rht*-MOF, the atomic point partial charges for each unique atom were determined from electronic structure calculations on representational gas phase fragments that mimic the chemical environment of the MOF as demonstrated in previous considerations.[68,70,71,79] More explicit details of this procedure can be found in the Supporting Information. The final calculated partial charges for each chemically distinct atom for all four *rht*-MOFs can also be found in Tables S1–S4 (see Supporting Information).

The charge fitting calculations on all four *rht*-MOFs revealed notable differences within the partial charges of the Cu^{2+} ions between *rht*-MOF-1 and MPAF-1 as well as between PCN-61 and Cu-TPBTM. In *rht*-MOF-1, the presence of the proximal negatively charged carbon-coordinated nitrogen atoms on the five-membered rings of the ligand causes the positive charge of the Cu1 ions to increase relative to the Cu2 ions. To put this in another perspective, this moiety causes the Cu1 ions in *rht*-MOF-1 to have the higher positive charge of the two Cu^{2+} ions through an inductive effect. In MPAF-1, however, the negatively charged carbon-coordinated nitrogen atoms are removed, as these atoms are replaced with a C—H group. Because these electronegative nitrogen atoms are vanished in MPAF-1, the Cu1 ions cannot increase in electron deficiency for this *rht*-MOF. As a result, the higher positive charge is localized to the Cu2 ions for MPAF-1 since these ions are located in a more favorable environment in general. Electronic structure calculations on all copper-containing fragments in PCN-61 revealed that the Cu2 ions have the greater charge in this *rht*-MOF. However, by substituting the nonpolar alkyne groups as observed in PCN-61 to the polar amide groups as seen in Cu-TPBTM, the electrostatic distribution about the Cu paddlewheels was reversed, as the presence of the electronegative oxygen atom of the amide group in Cu-TPBTM causes the partial positive charge of the Cu1 ions to increase.

Indeed, the quantum mechanical calculations showed that changing one atom or functional group in an *rht*-MOF can lead to different charge distributions about the Cu paddlewheels as demonstrated between rht-MOF-1 and MPAF-1 as well as between PCN-61 and Cu-TPBTM. This will result in different sorption mechanisms between the two pairs of *rht*-MOFs, as the Cu^{2+} ion that has the higher partial positive charge will be the preferred initial sorbate binding site. The results for the relative charge magnitudes about the Cu^{2+} ions of the paddlewheels for all four *rht*-MOFs are summarized in Figure 2.

Note, our parametrization of partial charges usually includes both fragment analysis and periodic charge fitting, where the electronic structure of the full MOF unit cell is considered.[100,107] The latter is computationally prohibitive due to the large unit cells involved; this is not strictly needed, however, given our experience with the established track record of fragment-based charge fitting.

The polarizable CO_2 potential used for the simulations in this work is a rigid five-site model that includes atomic point partial charges and point polarizability parameters on the atomic locations of the carbon and oxygen atoms.[85] The values for the partial charges and polarizabilities represent the molecular quadrupole and molecular polarizability tensor for CO_2, respectively. The C—O bond length for this CO_2 potential is 1.162 Å. Moreover, there are Lennard-Jones repulsion/dispersion parameters that are localized on the carbon atom and two phantom off-atomic sites that are positioned 1.114 Å from the carbon atom extending along the C_∞ axis. This model was parametrized according to a sorbate fitting procedure that was described previously.[84,108]

The TraPPE CO_2 model[89] was also used as a comparison to the aforementioned polarizable CO_2 model in this work. This model was chosen because of both its success as a bulk and liquid state potential and its wide adoption in sorption simulations. Specifically, the effects that implicit polarization have on the binding of CO_2 onto the open-metal sites in the *rht*-MOFs will be investigated using this potential. The TraPPE model is a rigid three-site model that includes Lennard-Jones parameters and point partial charges on the atomic locations of the carbon and oxygen atoms. The C—O bond distance is 1.160 Å for this model. It will be shown that simulations using the TraPPE model describe only a small quantity of CO_2 molecules about the open-metal sites in all four *rht*-MOFs as compared to the polarizable model. In addition, the Cu^{2+}-CO_2 distance is increased for simulations using the TraPPE model. The results obtained for all four *rht*-MOFs using the TraPPE model can be found in the SI. The parameters for the CO_2 models used in this work can also be found in the SI (Table S5). Note, both the polarizable and TraPPE CO_2 models can reproduce bulk CO_2 data (see Figure S6, SI). However, not surprisingly, only the polarizable model can accurately capture the proper sorption structure in a charged/polar MOF.

GCMC methods[109,110] were used to model CO_2 sorption in *rht*-MOF-1, MPAF-1, PCN-61, and Cu-TPBTM. More details of this method are described in the SI. Many-body polarization was imple-

mented using a Thole-Applequist type model,[70,78,97,111–114] which is also explained in the SI.

For *rht*-MOF-1 and MPAF-1, the simulations were performed in the respective unit cells where the nitrate ions are positioned in the corners of the truncated tetrahedral cages. Previous molecular dynamics (MD) simulation studies on these *rht*-MOFs have shown that these cages are the locations in which the nitrate ions migrate to in the dehydrated form of these MOFs at cold temperatures.[68,72] However, at ambient temperatures, the MD simulations showed that the nitrate ions exhibit mobility in these MOFs and they do not necessarily reside in these cages. Nevertheless, the aforementioned configuration was still used for the simulations in these two *rht*-MOFs since a model containing the estimated locations of the nitrate ions was required. The positions of the nitrate ions in *rht*-MOF-1 and MPAF-1 do not affect the metal paddlewheel sorption in these MOFs at low loading. The investigation of the interaction between the sorbate molecules and the Cu^{2+} ions of the paddlewheels is the main focus of this work.

The interactions between the CO_2 molecules and the Cu^{2+} ions for all four *rht*-MOFs were monitored using the radial distribution function, denoted $g(r)$. This quantity represents the probability of finding a CO_2 molecule at a certain distance from a Cu^{2+} ion. All simulations of CO_2 sorption within the four *rht*-MOFs were performed using the Massively Parallel Monte Carlo (MPMC) code,[115] which is currently available for download on GitHub.

2. Results and Discussion

GCMC simulations of CO_2 sorption were performed in *rht*-MOF-1, MPAF-1, PCN-61, and Cu-TPBTM using the polarizable potential at a variety of pressures at 298 K. Note, only the results at a low pressure are described in the main text since this is the regime where sorption onto the open-metal sites can be observed within the simulations as they are quickly saturated. Figures 3(a) and 3(b) show the radial distribution functions, $g(r)$, for the carbon atoms of the CO_2 molecules about the Cu1 ions (green colored Cu^{2+} ions in Figure 1; atom label 1 in Figure S2–S5) and Cu2 ions (yellow colored Cu^{2+} ions in Figure 1; atom label 2 in Figure S2–S5), respectively, for all four *rht*-MOFs at 298 K and 0.20 atm. Note, the radial distribution functions shown herein are normalized to a total magnitude of unity over the distance examined. This was chosen to obtain a direct comparison between the relative magnitudes about both types of Cu^{2+} ions as well as for each MOF.

A very large peak can be seen for the $g(r)$ about the Cu1 ions in *rht*-MOF-1 and Cu-TPBTM at a distance of 3.3 Å (Figure 3(a)). This peak corresponds to the loading of CO_2 molecules onto the Cu1 ions of the Cu paddlewheels in these *rht*-MOFs. The fact that this large peak was only seen for *rht*-MOF-1 and Cu-TPBTM demonstrates that the Cu1 ions are the dominant metal paddlewheel sorption sites in these two *rht*-MOFs at low loading, but not for MPAF-1 and PCN-61. This is due to the fact that the Cu1 ions have the higher partial positive charge in these two *rht*-MOFs. Indeed, the presence of the negatively charged carbon-coordinated tetrazolate nitrogen atoms and the negatively charged amide oxygen atoms in *rht*-MOF-1 and Cu-TPBTM, respectively, causes the Cu1 ions to become more positively charged and hence, directs the binding of CO_2 molecules onto those sites. Note, a higher peak can be seen about the Cu1 ions in *rht*-MOF-1 compared to Cu-TPBTM. This is because the positive charge of the Cu1 ion is greater for *rht*-MOF-1 relative to Cu-TPBTM. In contrast, simulations in MPAF-1 and PCN-61 showed a small occupation of CO_2 molecules about the Cu1 ions. In these *rht*-MOFs, the Cu1 ion has the lower positive charge of the two Cu^{2+} ions of the paddlewheels and thus, it interacts less strongly with the CO_2 molecules.

Though there were a few sorbed CO_2 molecules about the Cu1 ions in MPAF-1 and PCN-61, the simulations revealed that there were a significant occupation of CO_2 molecules about the Cu2 ions in these *rht*-MOFs. This was exemplified by the large peak at 3.3 Å for the $g(r)$ about the Cu2 ions in both of these *rht*-MOFs (Figure 3(b)). Both MPAF-1 and PCN-61 contain moieties on their respective ligands that are hydrophobic; thus, the Cu1 ions cannot become more positively charged in

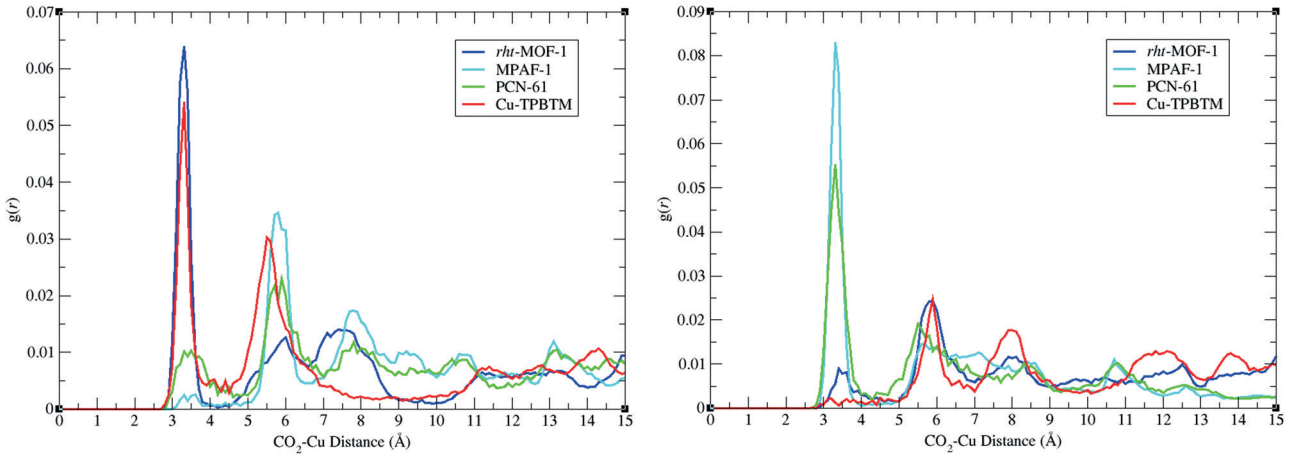

Figure 3. Radial distribution functions, $g(r)$, of CO_2 molecules about a) the Cu1 ions (green colored Cu^{2+} ions in Figure 1; atom label 1 in Figures S2–S5) and b) the Cu2 ions (yellow colored Cu^{2+} ions in Figure 1; atom label 2 in Figures S2–S5) using the polarizable CO_2 potential in *rht*-MOF-1 (blue), MPAF-1 (cyan), PCN-61 (green), and Cu-TPBTM (red) at 298 K and 0.20 atm.

these *rht*-MOFs due to the lack of proximal electron withdrawing groups. Rather, the higher positive charge for these *rht*-MOFs was localized to the Cu2 ions since these ions are located in what has been found to be a more favorable environment of the MOF (forming the joints of the cuboctahedral cages). Because the Cu2 ions have the higher partial positive charge in MPAF-1 and PCN-61, these ions become the preferred sorption sites about the metal paddlewheels for these two *rht*-MOFs at low loading. There is greater occupancy about the Cu2 ions in MPAF-1 compared to PCN-61 because the former contains the higher positive charge on that ion. As for *rht*-MOF-1 and Cu-TPBTM, there were only a small quantity of CO_2 molecules in the region of the Cu2 ions because the positive charge of these ions is lower compared to the Cu1 ions in these MOFs. Therefore, even though the Cu2 ions are located in a generally more favorable chemical environment in the MOF, the presence of the electronegative groups as seen in *rht*-MOF-1 and Cu-TPBTM causes the electron density to shift to the Cu2 ions, thus causing these ions to become less electron deficient (less positively charged) as they are the metals furthest removed from the electron-withdrawing groups (see Figure 2).

Although the $g(r)$ results about the Cu1 and Cu2 ions for all four *rht*-MOFs are shown for simulations at 298 K and 0.20 atm in the main text, analogous results for the $g(r)$ were also observed at other pressures. At lower pressures, the magnitude of the 3.3 Å radial distribution peak is mildly higher, whereas it is slightly reduced at higher pressures (see Figures S16–S19, SI). Note, the CO_2 carbon–Cu^{2+} ion distance observed for the *rht*-MOFs in this work is comparable to the corresponding distances that were observed in HKUST-1 via NPD and ab initio simulation studies (3.0–3.2 Å).[77]

Taking advantage of the feasibility of molecular modeling, simulations of CO_2 sorption were also performed in all four *rht*-MOFs where the partial charges of both Cu^{2+} ions of the Cu paddlewheel were artificially set to the same value; this also explicitly demonstrates how the electronics direct the sorption. For each *rht*-MOF, this was accomplished by averaging the calculated partial charges for the Cu1 and Cu2 ions and assigning this value as the point charge for all Cu^{2+} ions in the force field for the respective MOFs. This is a popular Cu paddlewheel parametrization that was used for the simulations in *rht*-MOFs in the past by other groups.[9,60,72,73] The results for these control simulations can be found in the SI (Figure S12). It can be seen that the 3.3 Å radial distribution peak about the Cu1 ions in *rht*-MOF-1 and Cu-TPBTM was reduced compared to the corresponding results from the normal force field. Similarly, this peak about the Cu2 ions in PCN-61 and MPAF-1 was smaller than the results from the respective derived potential energy surface for these *rht*-MOFs. When examining the 3.3 Å radial distribution peak about the Cu2 ions in *rht*-MOF-1 and Cu-TPBTM and the Cu1 ions in MPAF-1 and PCN-61 in their respective artificial force fields, the peaks were enhanced compared to the corresponding results for the normal case. However, a larger peak can still be seen about the Cu1 ions relative to the Cu2 ions for *rht*-MOF-1 and Cu-TPBTM, and likewise about the Cu2 ions relative to the Cu1 ions for MPAF-1 and PCN-61. This demonstrates that, even though the partial charges of the Cu^{2+} ions were constrained to be the same in these *rht*-MOFs, the simulations involving explicit polarization in these hypothetical potential energy surfaces still show that the Cu1 ions are the preferred metal paddlewheel binding sites for *rht*-MOF-1 and Cu-TPBTM and that the Cu2 ions are the preferred sites for MPAF-1 and PCN-61.

The simulated excess CO_2 sorption isotherms in PCN-61 and Cu-TPBTM at 298 K for the polarizable CO_2 potential and the TraPPE potential revealed isotherms in reasonably good agreement with the corresponding experimental data[48] for both models (see Figure S24, SI). However, in the case of the TraPPE model, good agreement with experiment does not necessarily correspond to capturing the most critical MOF-sorbate interactions in simulation as demonstrated below. Note, to the best of our knowledge, no experimental excess CO_2 sorption data is available for *rht*-MOF-1 and MPAF-1 for comparison to simulation.

The $g(r)$ results about the Cu1 ions in *rht*-MOF-1 and Cu-TPBTM as well as the Cu2 ions in MPAF-1 and PCN-61 for both the polarizable and TraPPE CO2 potentials are provided in the SI (Figure S11). In all cases, it was observed that the peak that represents sorption onto the open-metal sites was shifted to 3.6 Å for the TraPPE model, which is much farther away than the experimentally observed CO_2 carbon–Cu^{2+} distances for metal paddlewheel sorption.[77] Thus, for simulations using the TraPPE model, the CO_2 molecules do not sorb as closely to the Cu^{2+} ions compared to the simulations using the polarizable CO_2 potential. In addition, the nearest-neighbor peak about the Cu^{2+} ions for the TraPPE model was severely reduced relative to the polar CO_2 model. Thus, in addition to the shifted peak, the population of CO_2 molecules about the open-metal sites were reduced for simulations using the TraPPE model. The $g(r)$ results about the Cu1 and Cu2 ions for all four *rht*-MOFs using the TraPPE model at various pressures can be found in the SI (Figure S13–S14, S20–S23); the results are shown in the respective normal force fields for these *rht*-MOFs as well as cases where the charges of the two Cu^{2+} ions were constrained to equality.

Overall, these results demonstrate that the TraPPE model predictably does not describe the sorption of CO_2 molecules onto the open-metal sites as well as a model that accounts for explicit polarization. The Cu^{2+} ions in *rht*-MOFs are highly charged and polar and they require explicit induced dipole effects to capture the binding of sorbate molecules onto that site. A model that has only implicit polarization interactions, such as the TraPPE model is insufficient to capture the most salient sorbate-metal interaction. The majority of TraPPE CO_2 molecules can be found in the corners of the truncated tetrahedral cages for these *rht*-MOFs (see Figure S25, SI); these are regions that are dominated by van der Waals and charge–quadrupole interactions.

Simulations involving many-body polarization were used to determine the favorable sites of CO_2 sorption at initial loading in all four *rht*-MOFs. This was characterized by calculating the distribution of induced dipole magnitudes for the CO_2 molecules for the respective MOFs. The result is a plot of the dipole

magnitudes versus the normalized CO_2 population in the MOF.[19,70,71,78,116,117] The dipole distribution for a sorbate in a MOF contains a number of distinct peaks, with each peak correlating to a region of sorbate occupancy inside the MOF. A peak that is found at high dipole magnitudes usually corresponds to occupancy within the primary sorption sites in the MOF. In the case of most MOFs that contain open-metal sites, the preferred sorption sites are the metal centers.

Figure 4(a) shows the three-dimensional histograms displaying the regions of CO_2 occupancy about the Cu^{2+} ions of the metal paddlewheels in all four *rht*-MOFs. These histograms correlate to the highest dipole magnitude peak in the CO_2 dipole distribution for the respective MOFs. The three-dimensional histogram showing the sorption sites about the metal paddlewheels for *rht*-MOF-1 reveals that the CO_2 molecules sorb onto the Cu1 ions (the ions that project into the truncated tetrahedral and truncated octahedral cages) at initial loading. This is expected given that this MOF contains highly positively charged Cu1 ions as a result of the negatively charged tetrazolate nitrogen atoms of the tetrazolate moieties. In contrast, in MPAF-1, where the carbon-coordinated nitrogen atoms of the five-membered rings are replaced by C–H groups, the Cu1 ions are not the favored metal paddlewheel binding sites. Rather, the CO_2 sorption sites about the Cu paddlewheels are changed to the Cu2 ions (the ions that project into the cuboctahedral cages) in MPAF-1 as shown in the histogram for this MOF. Because the electronegative carbon-coordinated nitrogen atoms as seen in *rht*-MOF-1 are removed and replaced with hydrophobic C–H groups in MPAF-1, the Cu2 ions exhibit the higher positive charge in this *rht*-MOF and therefore, will interact with the CO_2 molecules more strongly.

In PCN-61, the three-dimensional histogram showing the population of CO_2 molecules about the open-metal sites reveals that the Cu2 ions are the preferred sorption sites in this MOF at low loading. PCN-61 shows a similar distribution of CO_2 molecule occupancy about the Cu2 ions as MPAF-1, which was expected since both *rht*-MOFs have the higher positive charge localized on the Cu2 ions due to the presence of hydrophobic groups on the organic linker. However, when the alkyne groups are replaced with amide groups as observed in Cu-TPBTM, the binding sites about the Cu paddlewheels are switched. In particular, the CO_2 molecules sorb onto the Cu1 ions in this MOF, similar to what was observed in *rht*-MOF-1, since the Cu1 ion has the higher positive charge of the two Cu^{2+} ions due to the presence of the nearby electronegative amide oxygen atom.

A close-up view of the CO_2 molecule orientation about the preferential Cu^{2+} ions of the Cu paddlewheels in all four *rht*-MOFs as captured from the Monte Carlo sorption history are shown in Figure 4(b). As demonstrated through the calculated

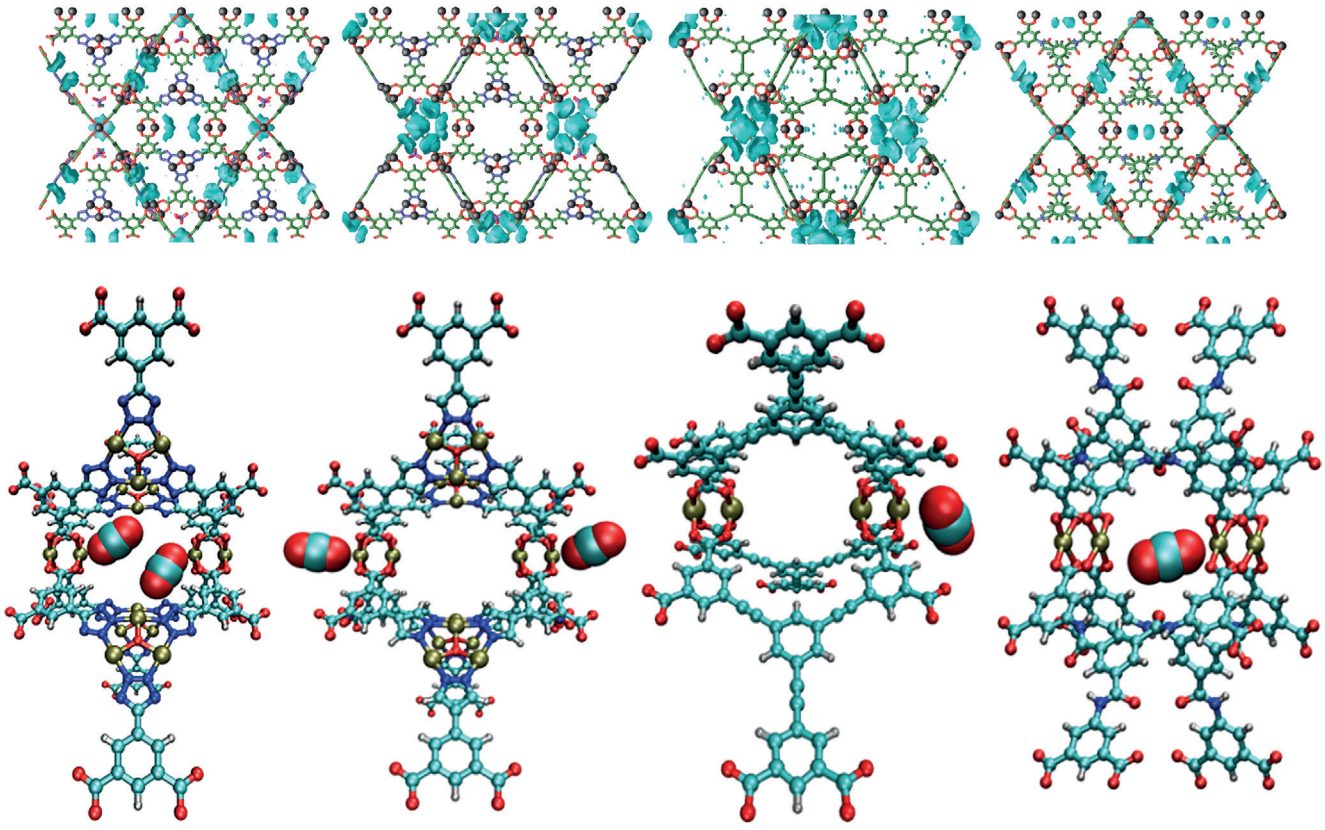

Figure 4. a) The three-dimensional histograms showing the initial CO_2 binding site (cyan) about the copper paddlewheels in *rht*-MOF-1, MPAF-1, PCN-61, and Cu-TPBTM. b) Molecular illustration of the CO_2 molecule binding site about the copper paddlewheels in *rht*-MOF-1, MPAF-1, PCN-61, and Cu-TPBTM. Atom colors: C = cyan, H = white, N = blue, O = red, Cu = tan.

partial charges for the two distinct Cu^{2+} ions, the radial distribution functions about both types of ions, and the three-dimensional histograms for all *rht*-MOFs, the CO_2 molecules sorb onto the Cu1 ions in *rht*-MOF-1 and Cu-TPBTM and the Cu2 ions in MPAF-1 and PCN-61.

Note, in *rht*-MOF-1, the void space between two adjacent Cu paddlewheels that are located on the edges of the respective cuboctahedral cages is large enough such that two CO_2 molecules can enter this region and each can coordinate to a Cu1 ion. In Cu-TPBTM, the pore sizes of the MOF are small such that only one CO_2 molecule can enter this region and bind to one of the Cu1 ions. However, as a result of this small space, the CO_2 molecule can orient itself such that one oxygen atom of the sorbate molecule can coordinate to one of the Cu1 ions and the other oxygen atom can nearly coordinate to the Cu1 ion of the adjacent Cu paddlewheel. This suggests the possibility of synthesizing an *rht*-MOF that can optimize this interaction for CO_2 binding. Specifically, an *rht*-MOF containing polar functional groups (to cause it to have a higher charge on Cu1) of appropriate dimensions can be constructed such that it exhibits even narrower pore sizes. By doing this, the CO_2 molecule can fit nicely between two Cu1 ions of the adjacent paddlewheels, with each CO_2 oxygen atom coordinating to a Cu1 ion. Indeed, this particular CO_2 molecule binding site was observed in Cu-TDPAT,[52,73,118] the smallest member of the *rht*-MOF family, through theoretical studies.[80]

3. Conclusions

In conclusion, we provided theoretical insights into how changing one functionality on the organic linker of *rht*-MOFs can lead to differences in the binding site about the metal paddlewheels. This was demonstrated by considering a series of MOFs from *rht*-MOF-1 to MPAF-1 and likewise from PCN-61 to Cu-TPBTM. In *rht*-MOF-1, the presence of the carbon-coordinared nitrogen atoms on the five-membered ring causes the Cu1 ions to increase in positive charge, and hence, direct sorption onto that site. In MPAF-1, the presence of the C–H groups in place of the nitrogen atoms on the five-membered ring as seen in *rht*-MOF-1 causes the Cu2 ions to increase in charge. Therefore, the Cu2 ions are the initial metal paddlewheel binding sites in this *rht*-MOF. In PCN-61, the organic linker contains nonpolar alkyne groups, which results in the Cu2 ion having the higher positive charge. Hence, like MPAF-1, the initial Cu paddlewheel sorption sites in PCN-61 are these Cu2 ion sites. However, as these alkyne groups are replaced with polar amide groups as observed in Cu-TPBTM, the presence of the amide oxygen atoms causes the Cu1 ions to increase in charge. Thus, in this *rht*-MOF, the initial binding sites about the metal paddlewheels are the Cu1 ions as in *rht*-MOF-1. The $g(r)$ about both types of Cu^{2+} ions produced from the molecular simulations involving explicit many-body polarization have confirmed these findings. A distinct peak at 3.3 Å, corresponding to sorption onto the open-metal sites of the Cu paddlewheels, can be seen about the Cu1 ions in *rht*-MOF-1 and Cu-TPBTM and about the Cu2 ions in MPAF-1 and PCN-61. Indeed, the *rht*-MOF platform is both tunable in the hexacarboxylate ligand and the Cu paddlewheel binding site, as the choice of functionality on the ligand can control the sorption about such sites as observed in this study.

Based on the results observed in this study, the initial Cu paddlewheel binding sites for other *rht*-MOFs can be predicted. For instance, in NTU-105,[60] and *rht*-MOF-4a,[56] it would be expected that the Cu1 ions will exhibit the higher positive charge in these *rht*-MOFs. This is due to the fact that these *rht*-MOFs contain polar functional groups on the linker (through 1,2,3-triazole and alkoxy groups, respectively) that will cause the Cu1 ions to increase in charge. Thus, it is predicted that the Cu1 ions would be the preferred initial sorption sites in these *rht*-MOFs. Overall, this study demonstrates both the tunable nature of the *rht*-MOF platform and the possibility for rational design of sorption and catalytic sites. Indeed, this study suggests the possibility for experimentalists to control desired binding sites in a MOF through aspirational chemical modifications in synthesis.

Supporting Information: Details of electronic structure calculations, many-body polarization overview, tables of properties, pictures of MOF fragments, details of simulation methods, and additional radial distribution functions and content.

Acknowledgements

This work was supported by the National Science Foundation (Award No. CHE-1152362). Computations were performed under an XSEDE Grant (No. TG-DMR090028) to B.S. This publication is also based on work supported by Award No. FIC/2010/06, made by King Abdullah University of Science and Technology (KAUST). The authors also thank the Space Foundation (Basic and Applied Research) for partial support. The authors would like to acknowledge the use of the services provided by Research Computing at the University of South Florida.

Keywords: copper · metal–organic frameworks · Monte Carlo simulations · partial charges · polarization

[1] O. M. Yaghi, H. Li, C. Davis, D. Richardson, T. L. Groy, *Acc. Chem. Res.* **1998**, *31*, 474–484.
[2] M. Eddaoudi, D. B. Moler, H. Li, B. Chen, T. M. Reineke, M. O'Keeffe, O. M. Yaghi, *Acc. Chem. Res.* **2001**, *34*, 319–330.
[3] M. Eddaoudi, J. Kim, N. Rosi, D. Vodak, J. Wachter, M. O'Keeffe, O. M. Yaghi, *Science* **2002**, *295*, 469–472.
[4] S. Kitagawa, R. Kitaura, S.-i. Noro, *Angew. Chem. Int. Ed.* **2004**, *43*, 2334–2375; *Angew. Chem.* **2004**, *116*, 2388–2430.
[5] J. R. Long, O. M. Yaghi, *Chem. Soc. Rev.* **2009**, *38*, 1213–1214.
[6] H.-C. Zhou, J. R. Long, O. M. Yaghi, *Chem. Rev.* **2012**, *112*, 673–674.
[7] D. J. Collins, S. Ma, H.-C. Zhou, *Metal-Organic Frameworks*, Wiley, Hoboken, **2010**, pp. 249–266.
[8] D. J. Collins, H.-C. Zhou, *J. Mater. Chem.* **2007**, *17*, 3154–3160.
[9] O. K. Farha, A. O. Yazaydin, I. Eryazici, C. D. Malliakas, B. G. Hauser, M. G. Kanatzidis, S. T. Nguyen, R. Q. Snurr, J. T. Hupp, *Nat. Chem.* **2010**, *2*, 944–948.
[10] D. M. D'Alessandro, B. Smit, J. R. Long, *Angew. Chem. Int. Ed.* **2010**, *49*, 6058–6082; *Angew. Chem.* **2010**, *122*, 6194–6219.
[11] T. M. McDonald, D. M. D'Alessandro, R. Krishna, J. R. Long, *Chem. Sci.* **2011**, *2*, 2022–2028.
[12] M. P. Suh, H. J. Park, T. K. Prasad, D.-W. Lim, *Chem. Rev.* **2012**, *112*, 782–835.

[13] K. Sumida, D. L. Rogow, J. A. Mason, T. M. McDonald, E. D. Bloch, Z. R. Herm, T.-H. Bae, J. R. Long, *Chem. Rev.* **2012**, *112*, 724 – 781.
[14] R. Q. Snurr, J. T. Hupp, S. T. Nguyen, *AIChE J.* **2004**, *50*, 1090 – 1095.
[15] J. A. Delgado, M. A. Uguina, J. M. Gmez, L. Ortega, *Sep. Purif. Technol.* **2006**, *48*, 223 – 228.
[16] J.-R. Li, Y. Ma, M. C. McCarthy, J. Sculley, J. Yu, H.-K. Jeong, P. B. Balbuena, H.-C. Zhou, *Coord. Chem. Rev.* **2011**, *255*, 1791 – 1823.
[17] J.-R. Li, J. Sculley, H.-C. Zhou, *Chem. Rev.* **2012**, *112*, 869 – 932.
[18] H. Wu, Q. Gong, D. H. Olson, J. Li, *Chem. Rev.* **2012**, *112*, 836 – 868.
[19] M. H. Mohamed, S. K. Elsaidi, L. Wojtas, T. Pham, K. A. Forrest, B. Tudor, B. Space, M. J. Zaworotko, *J. Am. Chem. Soc.* **2012**, *134*, 19556 – 19559.
[20] P. Nugent, Y. Belmabkhout, S. D. Burd, A. J. Cairns, R. Luebke, K. Forrest, T. Pham, S. Ma, B. Space, L. Wojtas, M. Eddaoudi, M. J. Zaworotko, *Nature* **2013**, *495*, 80 – 84.
[21] J. Lee, O. K. Farha, J. Roberts, K. A. Scheidt, S. T. Nguyen, J. T. Hupp, *Chem. Soc. Rev.* **2009**, *38*, 1450 – 1459.
[22] V. Lykourinou, Y. Chen, X.-S. Wang, L. Meng, T. Hoang, L.-J. Ming, R. L. Musselman, S. Ma, *J. Am. Chem. Soc.* **2011**, *133*, 10382 – 10385.
[23] M. Yoon, R. Srirambalaji, K. Kim, *Chem. Rev.* **2012**, *112*, 1196 – 1231.
[24] L. Meng, Q. Cheng, C. Kim, W.-Y. Gao, L. Wojtas, Y.-S. Chen, M. J. Zaworotko, X. P. Zhang, S. Ma, *Angew. Chem. Int. Ed.* **2012**, *51*, 10082 – 10085; *Angew. Chem.* **2012**, *124*, 10229 – 10232.
[25] X.-S. Wang, M. Chrzanowski, L. Wojtas, Y.-S. Chen, S. Ma, *Chem. Eur. J.* **2013**, *19*, 3297 – 3301.
[26] H. Xu, F. Liu, Y. Cui, B. Chen, G. Qian, *Chem. Commun.* **2011**, *47*, 3153 – 3155.
[27] Y. Cui, Y. Yue, G. Qian, B. Chen, *Chem. Rev.* **2012**, *112*, 1126 – 1162.
[28] L. E. Kreno, K. Leong, O. K. Farha, M. Allendorf, R. P. Van Duyne, J. T. Hupp, *Chem. Rev.* **2012**, *112*, 1105 – 1125.
[29] A. C. McKinlay, R. E. Morris, P. Horcajada, G. Férey, R. Gref, P. Couvreur, C. Serre, *Angew. Chem. Int. Ed.* **2010**, *49*, 6260 – 6266; *Angew. Chem.* **2010**, *122*, 6400 – 6406.
[30] P. Horcajada, R. Gref, T. Baati, P. K. Allan, G. Maurin, P. Couvreur, G. Férey, R. E. Morris, C. Serre, *Chem. Rev.* **2012**, *112*, 1232 – 1268.
[31] R. Ananthoji, J. F. Eubank, F. Nouar, H. Mouttaki, M. Eddaoudi, J. P. Harmon, *J. Mater. Chem.* **2011**, *21*, 9587 – 9594.
[32] M. Kurmoo, *Chem. Soc. Rev.* **2009**, *38*, 1353 – 1379.
[33] D.-F. Weng, Z.-M. Wang, S. Gao, *Chem. Soc. Rev.* **2011**, *40*, 3157 – 3181.
[34] M.-H. Zeng, Q.-X. Wang, Y.-X. Tan, S. Hu, H.-X. Zhao, L.-S. Long, M. Kurmoo, *J. Am. Chem. Soc.* **2010**, *132*, 2561 – 2563.
[35] G. Givaja, P. Amo-Ochoa, C. J. Gómez-García, F. Zamora, *Chem. Soc. Rev.* **2012**, *41*, 115 – 147.
[36] L. Croitor, E. B. Coropceanu, A. E. Masunov, H. J. Rivera-Jacquez, A. V. Siminel, M. S. Fonari, *J. Phys. Chem. C* **2014**, *118*, 9217 – 9227.
[37] E. Melnic, E. B. Coropceanu, O. V. Kulikova, A. V. Siminel, D. Anderson, H. J. Rivera-Jacquez, A. E. Masunov, M. S. Fonari, V. C. Kravtsov, *J. Phys. Chem. C* **2014**, *118*, 30087 – 30100.
[38] J. Yu, Y. Cui, C.-D. Wu, Y. Yang, B. Chen, G. Qian, *J. Am. Chem. Soc.* **2015**, *137*, 4026 – 4029.
[39] B. Moulton, M. Zaworotko, *Chem. Rev.* **2001**, *101*, 1629 – 1658.
[40] M. Eddaoudi, J. F. Eubank, *Metal-Organic Frameworks*, Wiley, Hoboken **2010**, pp. 37 – 89.
[41] F. Nouar, J. F. Eubank, T. Bousquet, L. Wojtas, M. J. Zaworotko, M. Eddaoudi, *J. Am. Chem. Soc.* **2008**, *130*, 1833 – 1835.
[42] Y. Zou, M. Park, S. Hong, M. S. Lah, *Chem. Commun.* **2008**, 2340 – 2342.
[43] Y. Yan, X. Lin, S. Yang, A. J. Blake, A. Dailly, N. R. Champness, P. Hubberstey, M. Schroder, *Chem. Commun.* **2009**, 1025 – 1027.
[44] S. Hong, M. Oh, M. Park, J. W. Yoon, J.-S. Chang, M. S. Lah, *Chem. Commun.* **2009**, 5397 – 5399.
[45] D. Zhao, D. Yuan, D. Sun, H.-C. Zhou, *J. Am. Chem. Soc.* **2009**, *131*, 9186 – 9188.
[46] D. Yuan, D. Zhao, D. Sun, H.-C. Zhou, *Angew. Chem. Int. Ed.* **2010**, *49*, 5357 – 5361; *Angew. Chem.* **2010**, *122*, 5485 – 5489.
[47] Y. Yan, I. Telepeni, S. Yang, X. Lin, W. Kockelmann, A. Dailly, A. J. Blake, W. Lewis, G. S. Walker, D. R. Allan, S. A. Barnett, N. R. Champness, M. Schröder, *J. Am. Chem. Soc.* **2010**, *132*, 4092 – 4094.
[48] B. Zheng, J. Bai, J. Duan, L. Wojtas, M. J. Zaworotko, *J. Am. Chem. Soc.* **2011**, *133*, 748 – 751.
[49] Y. Yan, A. J. Blake, W. Lewis, S. A. Barnett, A. Dailly, N. R. Champness, M. Schröder, *Chem. Eur. J.* **2011**, *17*, 11162 – 11170.
[50] Y. Yan, S. Yang, A. J. Blake, W. Lewis, E. Poirier, S. A. Barnett, N. R. Champness, M. Schroder, *Chem. Commun.* **2011**, *47*, 9995 – 9997.
[51] D. Yuan, D. Zhao, H.-C. Zhou, *Inorg. Chem.* **2011**, *50*, 10528 – 10530.
[52] B. Li, Z. Zhang, Y. Li, K. Yao, Y. Zhu, Z. Deng, F. Yang, X. J. Zhou, G. Li, H. Wu, N. Nijem, Y. J. Chabal, Z. Lai, Y. Han, Z. Shi, S. Feng, J. Li, *Angew. Chem. Int. Ed.* **2012**, *51*, 1412 – 1415; *Angew. Chem.* **2012**, *124*, 1441 – 1444.
[53] I. Eryazici, O. K. Farha, B. G. Hauser, A. O. Yazaydin, A. A. Sarjeant, S. T. Nguyen, J. T. Hupp, *Cryst. Growth Des.* **2012**, *12*, 1075 – 1080.
[54] B. Zheng, Z. Yang, J. Bai, Y. Li, S. Li, *Chem. Commun.* **2012**, *48*, 7025 – 7027.
[55] R. Luebke, J. F. Eubank, A. J. Cairns, Y. Belmabkhout, L. Wojtas, M. Eddaoudi, *Chem. Commun.* **2012**, *48*, 1455 – 1457.
[56] J. F. Eubank, F. Nouar, R. Luebke, A. J. Cairns, L. Wojtas, M. Alkordi, T. Bousquet, M. R. Hight, J. Eckert, J. P. Embs, P. A. Georgiev, M. Eddaoudi, *Angew. Chem. Int. Ed.* **2012**, *51*, 10099 – 10103; *Angew. Chem.* **2012**, *124*, 10246 – 10250.
[57] O. K. Farha, C. E. Wilmer, I. Eryazici, B. G. Hauser, P. A. Parilla, K. ONeill, A. A. Sarjeant, S. T. Nguyen, R. Q. Snurr, J. T. Hupp, *J. Am. Chem. Soc.* **2012**, *134*, 9860 – 9863.
[58] O. K. Farha, I. Eryazici, N. C. Jeong, B. G. Hauser, C. E. Wilmer, A. A. Sarjeant, R. Q. Snurr, S. T. Nguyen, A.. Yazaydn, J. T. Hupp, *J. Am. Chem. Soc.* **2012**, *134*, 15016 – 15021.
[59] X. Zhao, D. Sun, S. Yuan, S. Feng, R. Cao, D. Yuan, S. Wang, J. Dou, D. Sun, *Inorg. Chem.* **2012**, *51*, 10350 – 10355.
[60] X.-J. Wang, P.-Z. Li, Y. Chen, Q. Zhang, H. Zhang, X. X. Chan, R. Ganguly, Y. Li, J. Jiang, Y. Zhao, *Sci. Rep.* **2013**, *3*, 1149.
[61] C. E. Wilmer, O. K. Farha, T. Yildirim, I. Eryazici, V. Krungleviciute, A. A. Sarjeant, R. Q. Snurr, J. T. Hupp, *Energy Environ. Sci.* **2013**, *6*, 1158 – 1163.
[62] Y. Yan, M. Suyetin, E. Bichoutskaia, A. J. Blake, D. R. Allan, S. A. Barnett, M. Schröder, *Chem. Sci.* **2013**, *4*, 1731 – 1736.
[63] G. Barin, V. Krungleviciute, D. A. Gomez-Gualdron, A. A. Sarjeant, R. Q. Snurr, J. T. Hupp, T. Yildirim, O. K. Farha, *Chem. Mater.* **2014**, *26*, 1912 – 1917.
[64] R. Luebke, L. J. Weselinski, Y. Belmabkhout, Z. Chen, L. Wojtas, M. Eddaoudi, *Cryst. Growth Des.* **2014**, *14*, 414 – 418.
[65] X.-J. Wang, J. Li, P.-Z. Li, L.-B. Xing, H. Lu, H. Wu, Y. Shi, R. Zou, Y. Zhao, *Inorg. Chem. Commun.* **2014**, *46*, 13 – 16.
[66] K. Liu, B. Li, Y. Li, X. Li, F. Yang, G. Zeng, Y. Peng, Z. Zhang, G. Li, Z. Shi, S. Feng, D. Song, *Chem. Commun.* **2014**, *50*, 5031 – 5033.
[67] J. Li, P.-Z. Li, Q.-Y. Li, Y. Cao, H. Lu, H. Wu, F. Li, Y. Shi, X.-J. Wang, Y. Zhao, *RSC Adv.* **2014**, *4*, 53975 – 53980.
[68] W.-Y. Gao, R. Cai, T. Pham, K. A. Forrest, A. Hogan, P. Nugent, K. Williams, L. Wojtas, R. Luebke, L. J. Weselinski, M. J. Zaworotko, B. Space, Y.-S. Chen, M. Eddaoudi, X. Shi, S. Ma, *Chem. Mater.* **2015**, *27*, 2144 – 2151.
[69] X.-J. Wang, J. Li, Q.-Y. Li, P.-Z. Li, H. Lu, Q. Lao, R. Ni, Y. Shi, Y. Zhao, *CrystEngComm* **2015**, *17*, 4632 – 4636.
[70] K. A. Forrest, T. Pham, K. McLaughlin, J. L. Belof, A. C. Stern, M. J. Zaworotko, B. Space, *J. Phys. Chem. C* **2012**, *116*, 15538 – 15549.
[71] T. Pham, K. A. Forrest, P. Nugent, Y. Belmabkhout, R. Luebke, M. Eddaoudi, M. J. Zaworotko, B. Space, *J. Phys. Chem. C* **2013**, *117*, 9340 – 9354.
[72] R. Babarao, M. Eddaoudi, J. W. Jiang, *Langmuir* **2010**, *26*, 11196 – 11203.
[73] Z. Zhang, Z. Li, J. Li, *Langmuir* **2012**, *28*, 12122 – 12133.
[74] S. S.-Y. Chui, S. M.-F. Lo, J. P. H. Charmant, A. G. Orpen, I. D. Williams, *Science* **1999**, *283*, 1148 – 1150.
[75] V. K. Peterson, Y. Liu, C. M. Brown, C. J. Kepert, *J. Am. Chem. Soc.* **2006**, *128*, 15578 – 15579.
[76] C. M. Brown, Y. Liu, T. Yildirim, V. K. Peterson, C. J. Kepert, *Nanotechnology* **2009**, *20*, 204025.
[77] H. Wu, J. M. Simmons, G. Srinivas, W. Zhou, T. Yildirim, *J. Phys. Chem. Lett.* **2010**, *1*, 1946 – 1951.
[78] J. L. Belof, A. C. Stern, M. Eddaoudi, B. Space, *J. Am. Chem. Soc.* **2007**, *129*, 15202 – 15210.
[79] T. Pham, K. A. Forrest, A. Hogan, K. McLaughlin, J. L. Belof, J. Eckert, B. Space, *J. Mater. Chem. A* **2014**, *2*, 2088 – 2100.
[80] T. Pham, K. A. Forrest, J. Eckert, P. A. Georgiev, A. Mullen, R. Luebke, A. J. Cairns, Y. Belmabkhout, J. F. Eubank, K. McLaughlin, W. Lohstroh, M. Eddaoudi, B. Space, *J. Phys. Chem. C* **2014**, *118*, 439 – 456.

[81] T. Pham, K. A. Forrest, K. McLaughlin, J. Eckert, B. Space, *J. Phys. Chem. C* **2014**, *118*, 22683 – 22690.
[82] T. Pham, K. A. Forrest, R. Banerjee, G. Orcajo, J. Eckert, B. Space, *J. Phys. Chem. C* **2015**, *119*, 1078 – 1090.
[83] T. Pham, K. A. Forrest, A. Hogan, B. Tudor, K. McLaughlin, L. Belof, J. Eckert, B. Space, *Cryst. Growth Des.* **2015**, *15*, 1460 – 1471.
[84] J. L. Belof, A. C. Stern, B. Space, *J. Chem. Theory Comput.* **2008**, *4*, 1332 – 1337.
[85] A. L. Mullen, T. Pham, K. A. Forrest, C. R. Cioce, K. McLaughlin, B. Space, *J. Chem. Theory Comput.* **2013**, *9*, 5421 – 5429.
[86] C. R. Cioce, K. McLaughlin, J. L. Belof, B. Space, *J. Chem. Theory Comput.* **2013**, *9*, 5550 – 5557.
[87] K. Yu, J. G. McDaniel, J. Schmidt, *J. Phys. Chem. B* **2011**, *115*, 10054 – 10063.
[88] G. R. Medders, V. Babin, F. Paesani, *J. Chem. Theory Comput.* **2013**, *9*, 1103 – 1114.
[89] J. J. Potoff, J. I. Siepmann, *AIChE J.* **2001**, *47*, 1676 – 1682.
[90] T. Pham, K. A. Forrest, K. McDonald, B. Space, *Cryst. Growth Des.* **2014**, *14*, 5599 – 5607.
[91] A. K. Rappé, C. J. Casewit, K. S. Colwell, W. A. Goddard, W. M. Skiff, *J. Am. Chem. Soc.* **1992**, *114*, 10024 – 10035.
[92] Q. Yang, C. Zhong, J.-F. Chen, *J. Phys. Chem. C* **2008**, *112*, 1562 – 1569.
[93] T. Kawakami, S. Takamizawa, Y. Kitagawa, T. Maruta, W. Mori, K. Yamaguchi, *Polyhedron* **2001**, *20*, 1197 – 1206.
[94] T. Sagara, J. Klassen, E. Ganz, *J. Chem. Phys.* **2004**, *121*, 12543.
[95] G. Garberoglio, A. I. Skoulidas, J. K. Johnson, *J. Phys. Chem. B* **2005**, *109*, 13094 – 13103.
[96] J. L. Belof, A. C. Stern, B. Space, *J. Phys. Chem. C* **2009**, *113*, 9316 – 9320.
[97] P. T. van Duijnen, M. Swart, *J. Phys. Chem. A* **1998**, *102*, 2399 – 2407.
[98] R. DeVane, B. Space, A. Perry, C. Neipert, C. Ridley, T. Keyes, *J. Chem. Phys.* **2004**, *121*, 3688 – 3701.
[99] A. Perry, C. Neipert, B. Space, P. B. Moore, *Chem. Rev.* **2006**, *106*, 1234 – 1258.
[100] A. C. Stern, J. L. Belof, M. Eddaoudi, B. Space, *J. Chem. Phys.* **2012**, *136*, 034705.
[101] T. Pham, K. A. Forrest, K. McLaughlin, B. Tudor, P. Nugent, A. Hogan, A. Mullen, C. R. Cioce, M. J. Zaworotko, B. Space, *J. Phys. Chem. C* **2013**, *117*, 9970 – 9982.
[102] K. A. Forrest, T. Pham, A. Hogan, K. McLaughlin, B. Tudor, P. Nugent, S. D. Burd, A. Mullen, C. R. Cioce, L. Wojtas, M. J. Zaworotko, B. Space, *J. Phys. Chem. C* **2013**, *117*, 17687 – 17698.
[103] K. A. Forrest, T. Pham, P. Nugent, S. D. Burd, A. Mullen, L. Wojtas, M. J. Zaworotko, B. Space, *Cryst. Growth Des.* **2013**, *13*, 4542 – 4548.
[104] K. A. Forrest, T. Pham, K. McLaughlin, A. Hogan, B. Space, *Chem. Commun.* **2014**, *50*, 7283 – 7286.
[105] T. Pham, K. A. Forrest, P. A. Georgiev, W. Lohstroh, D. Xue, A. Hogan, M. Eddaoudi, B. Space, J. Eckert, *Chem. Commun.* **2014**, *50*, 14109 – 14112.
[106] J. Cirera, J. C. Sung, P. B. Howland, F. Paesani, *J. Chem. Phys.* **2012**, *137*, 054704.
[107] D.-L. Chen, A. C. Stern, B. Space, J. K. Johnson, *J. Phys. Chem. A* **2010**, *114*, 10225 – 10233.
[108] K. McLaughlin, C. R. Cioce, J. L. Belof, B. Space, *J. Chem. Phys.* **2012**, *136*, 194302.
[109] N. Metropolis, A. W. Rosenbluth, M. N. Rosenbluth, A. H. Teller, E. Teller, *J. Chem. Phys.* **1953**, *21*, 1087 – 1092.
[110] D. Frenkel, B. Smit, *Understanding Molecular Simulation: From Algorithms to Applications*, Academic Press, San Diego, **2001**.
[111] J. Applequist, J. R. Carl, K.-K. Fung, *J. Am. Chem. Soc.* **1972**, *94*, 2952 – 2960.
[112] B. Thole, *Chem. Phys.* **1981**, *59*, 341 – 350.
[113] K. A. Bode, J. Applequist, *J. Phys. Chem.* **1996**, *100*, 17820 – 17824.
[114] K. McLaughlin, C. R. Cioce, T. Pham, J. L. Belof, B. Space, *J. Chem. Phys.* **2013**, *139*, 184112.
[115] J. L. Belof, B. Space, *Massively Parallel Monte Carlo (MPMC)*, Available on GitHub, 2012, https://github.com/mpmccode/mpmc.
[116] P. Nugent, V. Rhodus, T. Pham, B. Tudor, K. Forrest, L. Wojtas, B. Space, M. Zaworotko, *Chem. Commun.* **2013**, *49*, 1606 – 1608.
[117] M. H. Mohamed, S. K. Elsaidi, T. Pham, K. A. Forrest, B. Tudor, L. Wojtas, B. Space, M. J. Zaworotko, *Chem. Commun.* **2013**, *49*, 9809 – 9811.
[118] H. Wu, K. Yao, Y. Zhu, B. Li, Z. Shi, R. Krishna, J. Li, *J. Phys. Chem. C* **2012**, *116*, 16609 – 16618.

Manuscript received: June 24, 2015
Final Article published: August 25, 2015